HiSST: International Conference on
High-Speed Vehicle Science Technology

26–29 November 2018, Moscow, Russia

Simulation of Pressure Gain Combustion in a Wave Rotor

P. R. Ess[1]

Abstract

In this paper the numerical study of constant volume combustion with associated pressure gain in a wave rotor configuration is presented. The setup was derived from conditions specified in the context of the project TREVAP, where future gas-turbine engines based on pressure-gain combustion of kerosene with air are investigated. In this work, a more sophisticated representation of the chemical reactions in the flow is employed than in the established literature for wave rotors. Because of the complexity of the combustion process in wave rotor based engines, strongly simplified simulations are performed. The two-dimensional simulations of reactive multi-species gas flow in a wave rotor contain up to twenty cycles in order to obtain a solution independent of transient start-up effects.
For the conditions defined, a first understanding of the combustion process and resulting flow and wave patterns is obtained. Further, the formation of pollutants was found to be significantly influenced by the high temperatures present in the wave rotor.
In the context of real engine operation, the issue of leakage was identified to be of potentially high importance, as the fuel-air mixture can penetrate into the areas around the wave rotor and cause problems with thermal load due to combustion.

Keywords: *Pressure gain combustion, wave rotor, combustion modelling.*

1. Introduction

When combustion occurs in a confined constant volume, the pressure will raise due to the heat release and the increase in temperature. This is called pressure-gain combustion and potentially offers a better efficiency in comparison to constant pressure combustion realised in conventional gas turbines. Three major configurations were identified in order to achieve pressure-gain combustion: combustion in a tube closed on one end producing a detonation wave, the rotating detonation wave and combustion in rotating channels. The latter is accomplished in the form of a wave rotor, which is one of the selected configurations in the project TREVAP. This project looks at future gas turbine engine concepts based on pressure-gain combustion. In this paper, the wave rotor is studied in a two-port configuration, shown in Fig. 1, and a basic understanding of the combustion processes within the given engine environment is developed.

The operation of the wave-rotor based aero-engine can be described as follows: As for a regular aero-engine, the air flows through the inlet into the compressor, where its pressure is increased due to the addition of work provided by the turbine. The compressed air is mixed with fuel and enters the wave rotor via the inlet port. The wave rotor is rotating at a well defined speed, so that the individual channels in the wave rotor become closed volumes. In those closed volumes combustion occurs, combined with a further increase in pressure. This is in contrast to the classical aero-engine, where constant pressure combustion occurs, associated with an increase in (fluid) volume. When the channel containing the burned high pressure gas rotates to the opening provided by the outlet port, the gas expands and enters the turbine, where work is extracted from the fluid for driving the compressor. After this, the gas can be expanded in a suitable nozzle. The requirement for effective pressure gain combustion is, that the pressure of the gas after leaving the wave rotor must be higher than the pressure entering the wave rotor. Further, the flow redirection from compressor to wave rotor as well as from wave rotor to

[1] *Institute for Combustion Technology, German Aerospace Center (DLR), Pfaffenwaldring 38-40, D-70569 Stuttgart, Germany, Email: peter.ess@dlr.de*

turbine must be taken care of, because the flows leaving the compressor and entering the turbine are circumferentially quite uniform, while the wave rotor inlet and outlet ports cover only a certain angle (c.f. Fig. 1).

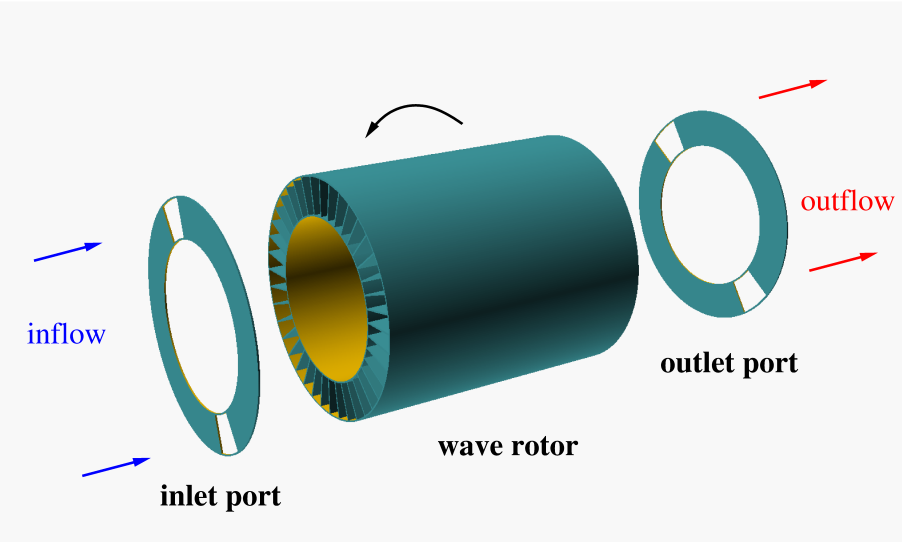

Fig 1. Geometry of wave rotor with dual inlet and outlet port configuration.

Extensive contributions with respect to combustion in wave rotors were made by Paxon, Nalim and co-authors. A numerical model for wave rotor analysis was presented by Paxon [9]. The model is based on one-dimensional inviscid flow computations and does not include chemical reaction in the flow. Nalim and Paxon [8] include the effects of chemistry by adding a simple chemistry model and associated transport processes in the gas. A review of wave rotor technology and its applications is given by Akbari et al. [7]. Further, Li et al. [5] and Nalim et al. [4] develop and present an air-standard aerothermodynamic analysis of gas turbine engines with wave rotor combustion. The model is simplified because combustion is realised as external heat addition to the gas.

The numerical simulation of constant volume combustion utilising kerosene as fuel and air as oxidator is of particular interest in this work, because previous works often used a limited presentation of the combustion. The modelling of chemical reaction processes can be realised with a simplistic approach, employing a one-way global reaction or highly sophisticated detailed chemical reaction schemes [15, 16]. The skeletal reaction scheme by Swithenbank et al. [1], employed in this work, lies within the two extremes.

The operation of the wave rotor is based on cycles, where each cycle corresponds to one revolution of the wave rotor for a machine with one port, or half a rotation in the two-port configuration investigated here. The concept follows works by Nalim et al. [4], with a combustion process based on a deflagration. Each cycle is divided into four phases, as described in Fig. 2. The phases are related to the specific port status: In phase A only the outlet port is open, in phase B both inlet- and outlet-ports, in phase C only the inlet port and, finally, in phase D both ports are closed during the constant volume combustion process.

2. Reference configuration

The reference configuration for the wave rotor is derived from assumptions, made for the overall configuration of the pressure gain combustion based future gas turbine engine devised in the project TREVAP [18].

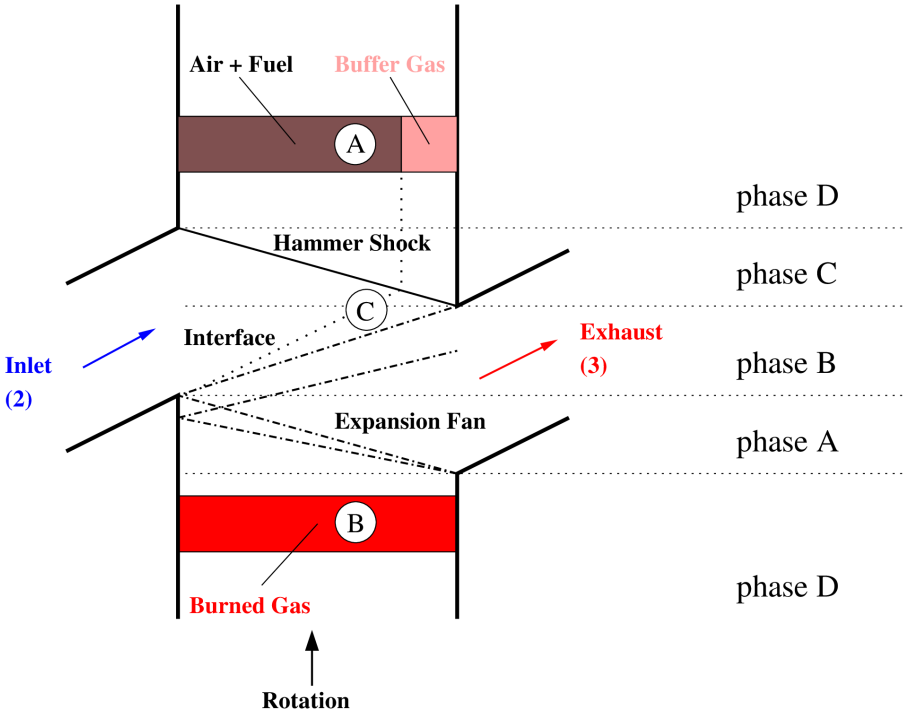

Fig 2. Scheme of wave rotor with phase definitions.

With respect to the wave rotor a number of main characteristics can be given: the wave rotor operates at 5000 rotations per minute in combination with a two-port configuration. Hence, the overall cycle time is $6\ ms$ and the phase times are given by 0.645, 0.055, 0.603 and $4.697ms$ for phases A, B, C and D, respectively (c.f. Fig. 2). The individual phase times for the configuration in this paper are given in Tab. 1 in combination with the port states. This yields overall opening times of $0.658\ ms$ for the inflow port and $0.7\ ms$ for the outlet port of the wave rotor. Based on the outcome of the flow computations

Table 1. *Phases for pressure-gain combustion in a wave rotor.*

phase	time, ms	inflow (left)	outflow (right)
A	0.645	closed	open
B	0.055	open	open
C	0.603	open	closed
D	4.697	closed	closed

shown in Section 4, an optimisation of the phase times would be possible. However, this is left for future work.

The inner and outer channel ring diameters are given with $0.1938m$ and $0.2895m$, respectively. Based on simplified turbulent flame speed calculations the wave rotor length was determined to $0.35\,m$. Details of the thermodynamic states prescribed as initial conditions for the wave rotor and derived from simplified thermodynamic analyses are given in Fig. 3. The mass flux at compressor exit is $27.642\ kg/s$, which increases due to fuel addition to $28.627\,kg/s$ at the entry to the turbine. This yields a fuel-to-air ratio of 0.0356. The fresh gas fill grade from the simplified calculations is approximately 28%, which corresponds

well with the results from the two-dimensional calculations presented in the following section. With the present setup, the inlet pressure of $9.0\,MPa$ is increased to $13.4\,MPa$ at the outlet port.

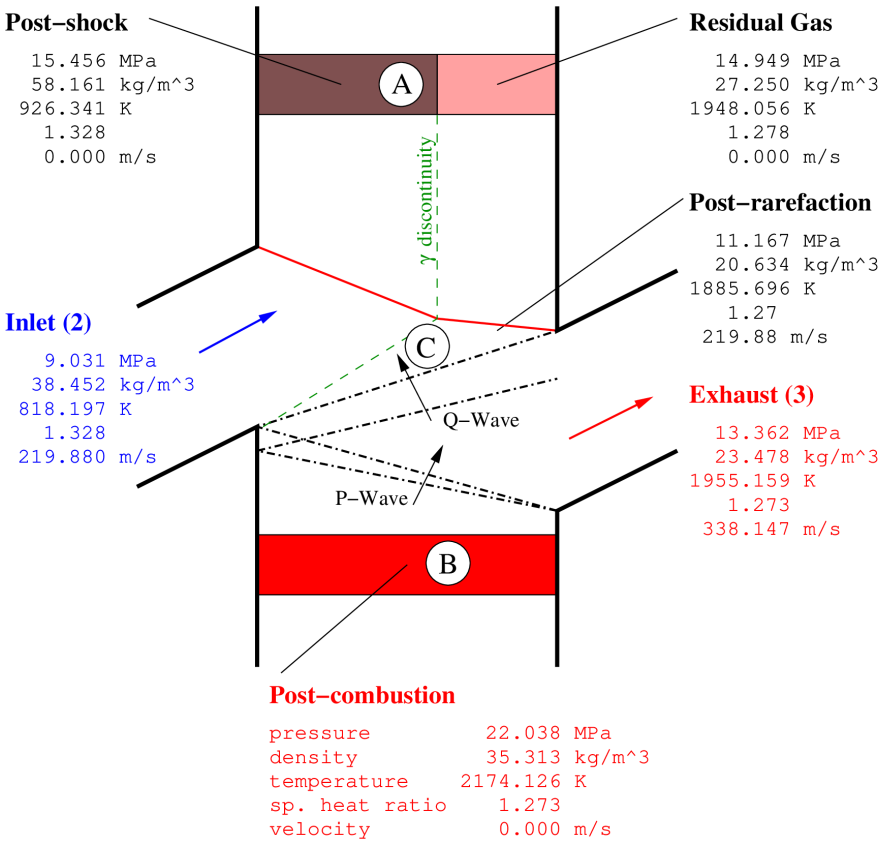

Fig 3. Combustion wave rotor with initial state based on data specified in the project TREVAP [18] (Inlet) and analytical calculations for all other states.

3. Species properties and reaction schemes

3.1. Modelling of kerosene combustion

Because kerosene is a mixture of a larger number of hydrocarbons, accurate modelling of its combustion is complex and requires large chemical reaction schemes employing a large number of species. An example is the scheme by Slavinskaya et al. [3], containing 1635 reactions for 244 species. Such a scheme increases the computational cost of flow simulations to a point, where they are not feasible any more. Therefore, complex flow simulations are performed employing strongly reduced schemes, where the kerosene is represented in the form of a surrogate fuel, containing only a few well chosen hydrocarbons. Typically, the ratio of carbon to hydrogen atoms in the surrogate is equal or close to that of kerosene. The reduced reaction schemes based on the surrogate fuel can then be compared with the complex schemes with a more realistic representation of kerosene. This can be done by investigating ignition delay times in the form of zero-dimensional computations. In the following, the species properties are given, before such a validation of the reduced reaction schemes used for the work are compared in terms of ignition delay times.

The chemical reaction schemes for kerosene-air combustion published by Swithenbank et al. [1] and Wang [2] are considered in this work and discussed briefly in the following. The scheme by Swithenbank et al. contains 17 reactions for the 13 species H, O, H_2, OH, CO, O_2, H_2O, CO_2, $C_{12}H_{24}$, N, NO,

N_2O and N_2. The consumption of kerosene, represented by $C_{12}H_{24}$, is described by a single one-way reaction. This simplifies the kinetic scheme strongly.

The scheme by Wang contains 14 reactions and 10 species, treating nitrogen as inert species. The species involved are H, O, H_2, OH, CO, O_2, H_2O, CO_2, $C_{12}H_{24}$ and N_2. The consumption of kerosene, again, represented in the form of $C_{12}H_{24}$, is modelled with two one-way reactions. One of them is based on the combustion of paraffin and the other on that of naphthene. Soot formation and soot oxidation, which are also part of the original scheme by Wang, are neglected in this work.

In both small scale schemes by Swithenbank et al. and Wang, $C_{12}H_{24}$ is taken as a surrogate fuel [2] to resemble the features of kerosene without the complexity introduced in calculations by an inclusion of all different species real kerosene is composed of. In correspondence to the two one-way reactions in Wang's scheme, the surrogate is created as a blend of paraffins and naphthenes, with 41.7 % and 58.3 % volume share, respectively. The thermodynamic coefficients for the computation of specific heat capacity, enthalpy and entropy of the surrogate are calculated from the corresponding data for paraffins and naphthenes.

The kerosene surrogate defined by Wang [2] differs from the cyclo-dodecan, which is represented by the same formula $C_{12}H_{24}$ used for the surrogate. The kerosene surrogate of the scheme by Slavinskaya et al. consists of the species $C_{10}H_{22}$, C_8H_{18} and C_7H_8 with a composition in terms of molar fractions of 0.65, 0.23 and 0.12, respectively, or in terms of mass fractions 0.7124, 0.2024 and 0.0852.

The thermodynamic data for the species are taken from publications of McBride et al. [10] as well as Goos et al. [11]. In this standard approach specific heat, enthalpy and entropy are represented by polynomials of fifth order for a low and a high temperature range, typically covering a range from $200\,K$ up to $6000\,K$. Transport properties for the species are obtained by means of kinetic gas theory using data provided by Hirschfelder et al. [12], Gardiner [13] and Chae [14].

3.2. Properties of reactants and combustion products

Before the given data are used for an analysis of the processes in the wave rotor, a look at thermodynamic data of the major species is taken. The global reaction

$$aC_xH_y + bO_2 + cN_2 \rightarrow axCO_2 + \frac{1}{2}ayH_2O + \left[b - a\left(x + \frac{1}{4}y\right)\right]O_2 + cN_2 \tag{1}$$

is considered for lean fuel-air mixtures. For stoichiometric mixtures oxygen would be consumed completely. Here, x equals 12 and y equals 24 in order to model the $C_{12}H_{24}$ kerosene surrogate and the ratio of oxygen to nitrogen in air in terms of moles is given by b/c as $1/3.76$. This yields

$$aC_{12}H_{24} + bO_2 + 3.76bN_2 \rightarrow 12aCO_2 + 12aH_2O + (b - 18a)\,O_2 + 3.76bN_2 \tag{2}$$

and it is easy to see, that for $b = 18a$ a stoichiometric mixture can be obtained. In Tab. 2 the species molar and mass fractions for reactants and products for complete combustion are given for the stoichiometric and a reference case. This reference case features a fuel fraction specified in the TREVAP configuration [18]. The table is given for the major species. As soon as minor species, e.g. radicals such as C, H, CO or OH, are present, the mass fractions of the major species would be smaller than those given in the table. For the hydrocarbon system considered, the total number of moles increases during the combustion process.

In Fig. 4 specific heats and specific heat ratios are shown for reactants and products at stoichiometric and lean conditions as well as for pure air. The lean mixture contains marginally more than half the molar amount of fuel as the stoichiometric mixture does and defines the reference setup. The impact of fuel is very noticeable, as the specific heat is significantly higher for a higher amount of fuel in the mixture. As a consequence, the specific heat ratio is much lower for the stoichiometric versus the lean fuel mixture. For the temperature range from $800\,K$ to $2500\,K$, the specific heat ratio deviates significantly from the assumptions made by Nalim et al. [4], when considering more realistic multi-species gas flow.

Table 2. Reactants (upper part) and products (lower part) for complete combustion of $C_{12}H_{24}$ for stoichiometric conditions and the conditions specified in the project TREVAP.

species	M_i	stoichiometric			reference		
		n_i	X_i	Y_i	n_i	X_i	Y_i
	$\frac{kg}{kmol}$	$kmol$			$kmol$		
$C_{12}H_{24}$	168	1.00	0.011537	0.063661	0.5228	0.006065	0.034325
O_2	32	18.00	0.207660	0.218261	18.0000	0.208810	0.225099
N_2	28	67.68	0.780803	0.718079	67.6800	0.785125	0.740576
$\sum$		86.68	1.000000	1.000000	86.2028	1.000000	1.000000
$\overline{M}$		30.445778 $kg/kmol$			29.684.307 $kg/kmol$		
CO_2	44	12.00	0.130890	0.200073	6.2736	0.070635	0.107875
H_2O	18	12.00	0.130890	0.081848	6.2736	0.070635	0.044131
O_2	32	0.00	0.000000	0.000000	8.5896	0.096711	0.107417
N_2	28	67.68	0.738220	0.718079	67.6800	0.762018	0.740577
$\sum$		91.68	1.000000	1.000000	88.8168	1.000000	1.000000
$\overline{M}$		28.785340 $kg/kmol$			28.810657 $kg/kmol$		

A further point of interest is the representation of kerosene in the multi-species gas environment and the combustion process. In Fig. 5 the kerosene surrogate proposend by Wang [2] is compared to Jet-A and cyclo-dodecane data of Goos et al. [11]. The surrogate behaves very similar to Jet-A and slightly differs from the cyclo-dodecane. At the same time, the surrogate formally has the same molecular weight and chemical formula, $C_{12}H_{24}$, as cyclo-dodecane.

3.3. Ignition delay times

With the framework for the species, their thermodynamic properties and the chemical reaction schemes introduced, the behaviour of the reaction schemes in terms of ignition delay time is compared in the following. The initial conditions for pressure and temperature, $11\ MPa$ and $840\ K$, respectively, correspond to a state between inflow and post-hammer-shock conditions obtained from analytical calculation presented later in Fig.3. In terms of pressure and temperature this is slightly less than what would be obtained as a state after the hammer shock. Any other state observed for reactants in the wave rotor would lead to faster ignition. The fuel-air mixture is derived from the stoichiometric composition of the surrogate fuel with air. The fuel used in the large reaction scheme by Slavinskaya et al. differs in the ratio of carbon to hydrogen atoms and thus in reaction enthalpy, compared to the present one. Therefore, the amount of fuel for computations using the large reaction scheme is chosen to yield an equivalent amount of air mass fraction in the gas mixture.

In general, depending on the pressure and temperature present, differences between reduced and more evolved chemical reaction schemes must be expected. The more reduced a reaction scheme is, the more restricted its area of application will be. Considering the ignition delay time, the one-way reactions in the reduced schemes are conveniently accessible to adjustments. The reaction progress of the one-way reactions is based on an extended Arrhenius formulation with some additional adjustments, e.g. in order to account for specific species concentrations and pressure. In the case of the scheme by Wang, this

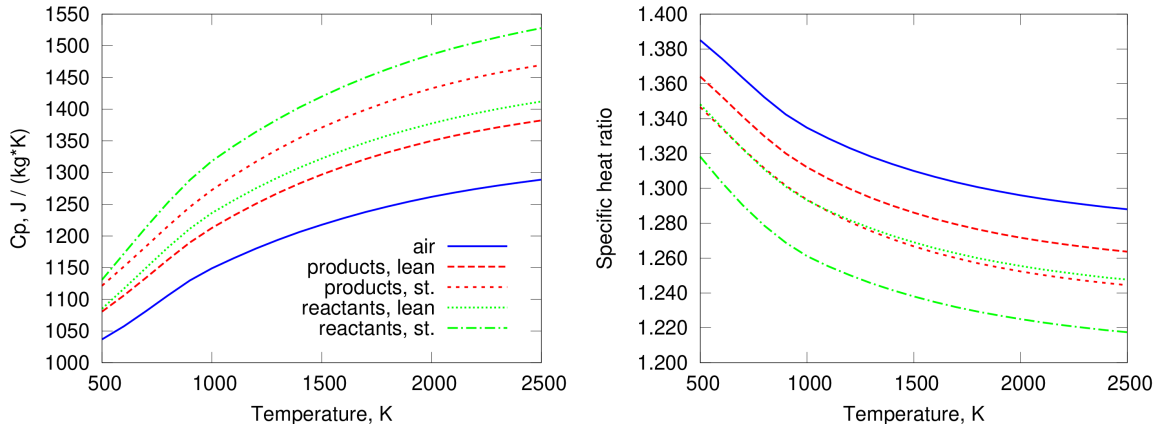

(a) Specific heat. (b) Specific heat ratio.

Fig 4. Gas properties for air, fuel-air mixtures and products.

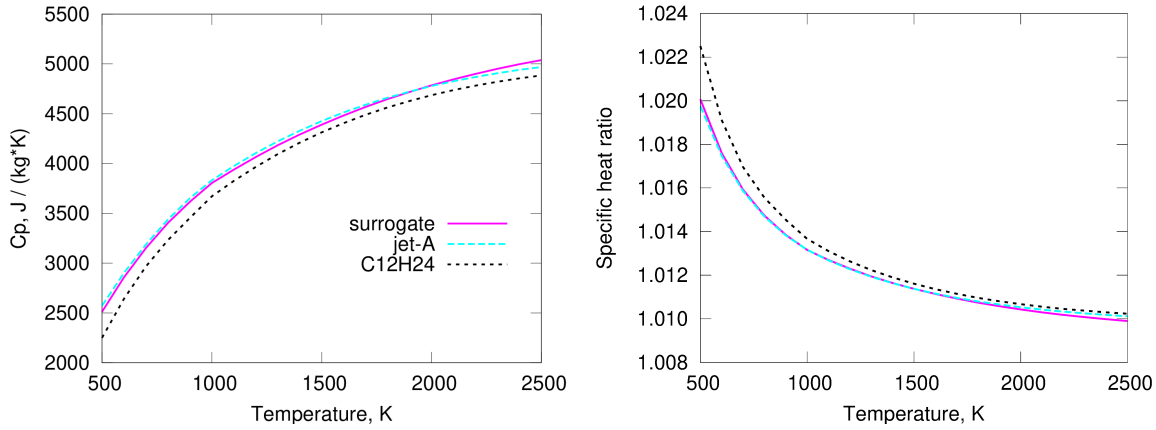

(a) Specific heat. (b) Specific heat ratio.

Fig 5. Gas properties for kerosene: surrogate, jet-A and $C_{12}H_{24}$.

reads

$$-\frac{d\,[C_{12}H_{24}]}{dt} = \underbrace{A \times T^{B} \times \exp\left(-\frac{E_a}{R_m T}\right)}_{\text{Arrhenius equation}} \times [C_{12}H_{24}]^{0.5} \times [O_2] \times p^{0.3} \tag{3}$$

with A as reaction coefficient, B as exponent of temperature T and E_a as activation energy. The gas constant is given by R_m, concentrations in square brackets and the pressure by p.

In its original form the scheme by Wang predicts ignition to occur much faster than the other schemes. With a variation of the coefficient A, the solution of the reduced scheme can be moved towards the reference solution. Here, a reduction of A by a factor of 60 in the forward reaction rate computation was applied. As can be seen in Fig. 6 a), the profile of the temperature, in particular the quick raise at the moment of ignition, for the adjusted scheme by Wang is very similar to the behaviour of the large scheme by Slavinskaya et al.

When the ignition delay of the large reaction scheme is taken as reference, the scheme by Swithenbank et al. can be taken in its original form and the scheme by Wang is used in the modified form. This yields the temperature profiles also shown in Fig. 6 a). The differences of the scheme by Swithenbank

et al. in its original form and in the form, when reactions with nitrogen-containing species are removed, are marginal. The agreement over a larger temperature range is still good, however, showing some discrepancies.

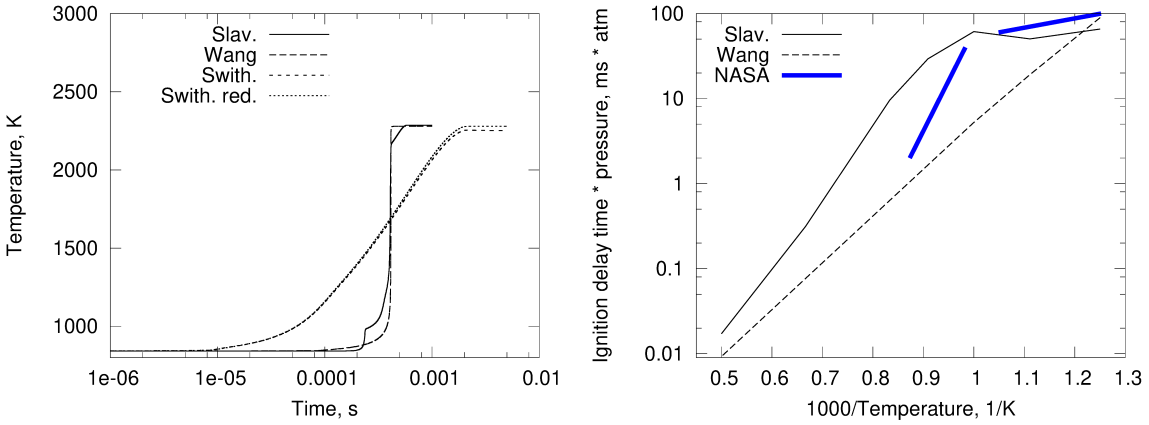

(a) Evolution of temperature.

(b) Ignition delay times.

Fig 6. Temporal evolution of temperature and ignition delay times for selected reaction schemes. The temporal evolution is given for initial conditions specified as $840\,K$ and $11\,MPa$. The reference data for *NASA* is taken from Lefebvre et al. [17]

For the sophisticated scheme by Slavinskaya et al. and the adjusted scheme by Wang, the ignition delay times over a range of initial temperatures different from the initial conditions introduced before, are shown in Fig. 6 b). Both schemes differ in particular in the low-temperature regime, where the larger scheme by Slavinskaya et al. does show a non-continuous behaviour and follows data by Lefebvre et al. [17] quite well. However, the overall trends for both schemes agree well, and the ignition delay time for all schemes for the initial conditions present in the wave rotor setup agree well. This holds, especially when considering typical data for ignition delay times from different sources, where substantial differences can be found in measurements due to, e.g. measurement procedures or the pressure applied in the experiment.

One essential consequence of the ignition delay times obtained for all relevant reaction schemes for the given temperature and pressure range is, that chemical reaction is very fast in comparison to the operating conditions devised for the wave rotor. Premature ignition in premixed fuel-air mixtures must be expected to be more of a relevant problem than the potential lack of ignition.

Also, it is important to keep in mind that the reduced and partially adjusted small reaction schemes were only compared in terms of ignition delay times. The composition of kerosene differs and, further, no statement in terms of combustion products has been made. Despite this, the initial and final temperatures are in agreement. With respect to an analysis of the wave rotor in terms of thermo-chemical behaviour the reduced schemes should be sufficient, but in terms of an analysis of combustion pollutants limitations must be accepted.

4. Setup of two-dimensional simulation

The governing equations for the fluid flow under consideration are the reactive multi-species Navier-Stokes equations. While some analyses concerning wall boundary layers and heat flow use the full set of equations, the main results presented here are based on the inviscid equations for reactive multi-species gas flows. This is sufficient to capture the gas dynamics and chemical reactions in wave rotor operation. In this way, substantial computational effort and cost required for an accurate representation of all boundary layer effects is avoided. The solutions of model problems corresponding to the proposed wave

rotor configuration have indicated, that boundary layers are very small, requiring near wall resolutions of below $1\ \mu m$. Uncertainties and simplifications applied in the present framework do not justify such excessive additional effort at this state.

The flow within the wave rotor is highly unsteady, with pressure waves being reflected at the walls and potentially propagating upstream or downstream, provided the respective ports around the wave rotor are open. It is difficult to implement boundary conditions directly at the inflow and outflow ports of the wave rotor, because in reality there is a space between compressor and wave rotor as well as between wave rotor and turbine. Hence, it must be expected that pressure waves propagate into the reservoir spaces defined by the volume between compressor, wave rotor and turbine.

In reality, compressor, wave rotor and turbine are all dynamically linked, i.e. the compressor is driven by work obtained from the turbine, which is able to extract work from the fluid compressed before, because combustion added chemical bond energy to the fluid in form of heat. The accurate simulation of this flow and reaction process by computational fluid dynamics may be performed, once the basic principles are well understood. Therefore, strong simplifications are made in order to gain a sufficient understanding of the behaviour of the wave rotor. As shown in Fig. 7, the wave rotor is augmented with a reservoir on both inflow and outflow sides. While the state after the last compressor stage is prescribed as inflow to the respective reservoir, the reservoir at the outflow side contains a nozzle.

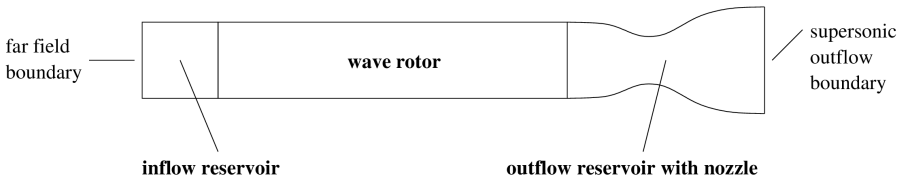

Fig 7. Wave rotor with reservoirs.

The nozzle throat can be varied in size. This effectively introduces a channel blockage and, in combination with the ambient pressure prescribed at the outflow plane of the reservoir, results in supersonic flow in the diverging part of the nozzle. Hence, a well defined boundary condition based on the critical flow condition at the nozzle throat is introduced, where the size of the smallest cross section of the nozzle can be adjusted to regulate the mass flow through the wave rotor. In the present case, the nozzle throat height is $58\,\%$ of the channel height. In this way the resulting mass flux corresponds well with the value given by the analytical cycle calculation.

This nozzle arrangement is thought to emulate a turbine, where the exact flow conditions are not known. However, a first turbine stage might contain a cross section with critical flow, similar to that defined by the carefully adjusted outflow reservoir.

An important aspect during multiple cycle calculations is how data are being reused during the computations. While data within the wave rotor obtained at the end of one phase are being reused as starting condition for the computation of the next phase, a more elaborate scheme is required for inflow and outflow reservoir data. Because inflow and outflow reservoirs are only relevant, when the inlet and outlet ports are open, respectively, reservoir data from a previous phase must be reused, when a port is just being opened. How this is accomplished, is visualised in Fig. 8. The green arrows symbolise, where data from one phase are being used as initial conditions for the next phase the arrows lead to. For instance, in the case of the wave rotor, data from the previous phase are always directly used for the next phase. In the case of the inlet reservoir, data from phase B are used as initial conditions for phase C, and then data from phase C are used as initial condition for phase B of the next cycle. The outflow reservoir follows the same pattern, however, applied to phases A and B.

After a sufficiently high number of cycles, the transient from the start up can be removed and the flow in the inlet and outlet port reservoirs is periodic. From this point on the solution remains the same for the following cycles, however, it must be kept in mind that it does not fully correspond to a solution that

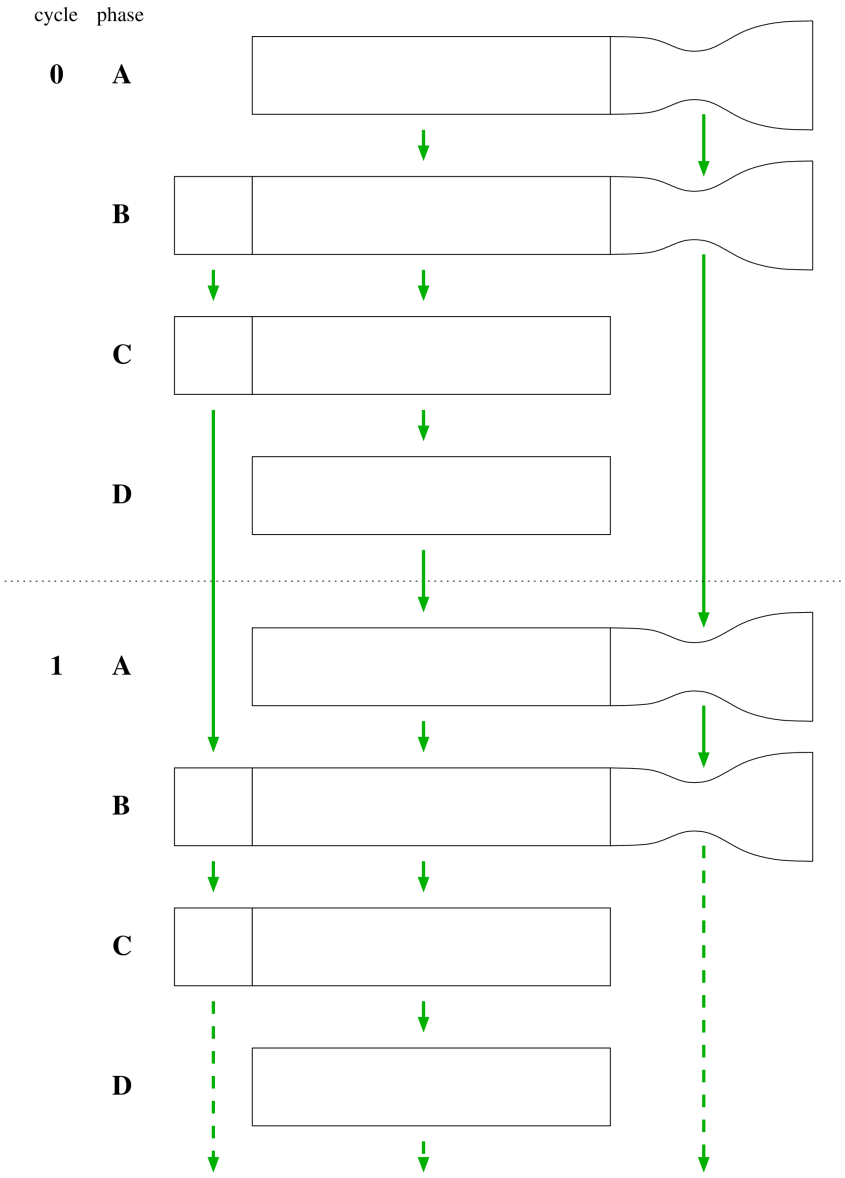

Fig 8. Data reusage scheme for computation of multiple cylces. The green arrows symbolise, where data from one phase are being used as initial conditions for the next phase the arrows lead to.

would be obtained from a fully three-dimensional simulation. In a fully three-dimensional simulation there would be significant flow induced in circumferential direction complicating the overall flow field and non-uniformity of the flow significantly.

A perfectly premixed fuel-air gas is presumed at the inlet and the fuel injection, vaporisation and mixing processes are not included here to avoid excessive complexity when studying the basic functionality of the proposed engine concept. This simplification is considered acceptable, because at the high inflow temperature above $800\,K$ specified in this work, vaporisation should not be an issue if the fuel is injected using the standard tools employed in present aero-engines. At the same time, it is worth paying attention to the fuel injection and mixing process in order to address the very short ignition delay time resulting under the given conditions. It might be useful to deliberately delay or extend the ignition and combustion processes for better combustion control. However, this is left for future work. In the present numerical study the combustion is effectively restricted to phase D. Any combustion occurring in the plenum before

the wave rotor would be very problematic.

5. Results

The computations of chemically reacting flow are performed on two-dimensional grids, containing from $3\,k$ to $0.275\,M$ cells, where the domain is defined by the wave rotor as well as an inflow- and outflow reservoir. The outflow reservoir features a nozzle to allow for an adjustment of the mass flow, which resembles the effect of the first turbine stage in the real engine. Further, the wave rotor is characterised by a dual port configuration, a length of $0.35\,m$ and a cycle duration of $6\,ms$.

Depending on the configuration, the transient from the start of the solution procedure is removed after 10 to 20 cycles. Hence, at this state a converged cycle operation is reached.

The results in the next two subsections, general findings and pollutant formation, are presented in terms of cross-section averaged values. While for the pressure area based averages are calculated, for temperature and species mass fractions mass flux based averages are computed. The implications of wave rotor leakage are demonstrated by showning the full two-dimensional flow field. While the calculations containing up to 20 cycles were performed on the grids with smaller cell numbers, the calculations used to study the leakage effects were performed on a grid with much higher cell numbers.

5.1. General findings

The simulated pressure and temperature fields during a converged cycle operation are shown in Fig. 9. Interesting flow features are the rarefaction wave that originates from the outflow boundary and propagates upstream during phase A. At the beginning of phase C the hammer shock is generated, again at the outflow port due to its instantaneous closure. The hammer shock propagates upstream and, with the given duration of phase C, it even propagates into the inflow reservoir. More fine-tuned phase times might be appropriate in order to avoid this effect and retain the effect of the pressure rise in the wave rotor. This would imply reducing the duration of phase C.

The temperature field shows the low temperature inflow gas, propagating into the wave rotor. With the prescribed timing approximately one third of the wave rotor is filled with fresh gas, which is in agreement with assumptions made by the project partners in their cycle calculation. As combustion is switched on in phase D, the fresh gas is consumed within approximately $3\,ms$, which is less than the time allocated for phase D. However, due to the uncertainties with respect to the combustion process during real wave rotor operation, the allocation of this surplus time is reasonable. Aside from combustion, the flow during phase D is characterised by pressure waves repeatedly propagating from one side of the wave rotor to the other and back.

Figure 10 shows the evolution of pressure, temperature and mass fluxes at inlet and outlet ports during a complete cycle. The effects of rarefaction wave during phase A and B, hammer shock during phase C and the repeatedly reflected pressure waves during phase D can be observed in the pressure history in Fig. 10 (a). The plot for the temperature in Fig. 10 (b) clearly shows the low temperature of the premixed gas entering though the inflow port, as well as the gradual increase on temperature due to combustion during phase D. The temperature is affected by the pressure waves as well, however, with an upper level of approximately $2200\,K$ being reached. The mass flux given in Fig. 10 (c) illustrates the outflow during phases A and B and the inflow during phases B and C. The small peaks in mass flux at inflow and outflow boundaries during phase D are due to the fact, that the mass flux is not measured exactly at the boundary, where it should be zero, but at the first and last interior cell of the computational domain. The fuel mass fraction given in the last graph of Fig. 10 (d) shows the consumption of fuel over time. Again, there is the strong indication for the given flow conditions, that $3\,ms$ are more than sufficient to consume all fuel. The remaining time spent during phase D is effectively wasted from a combustion point of view.

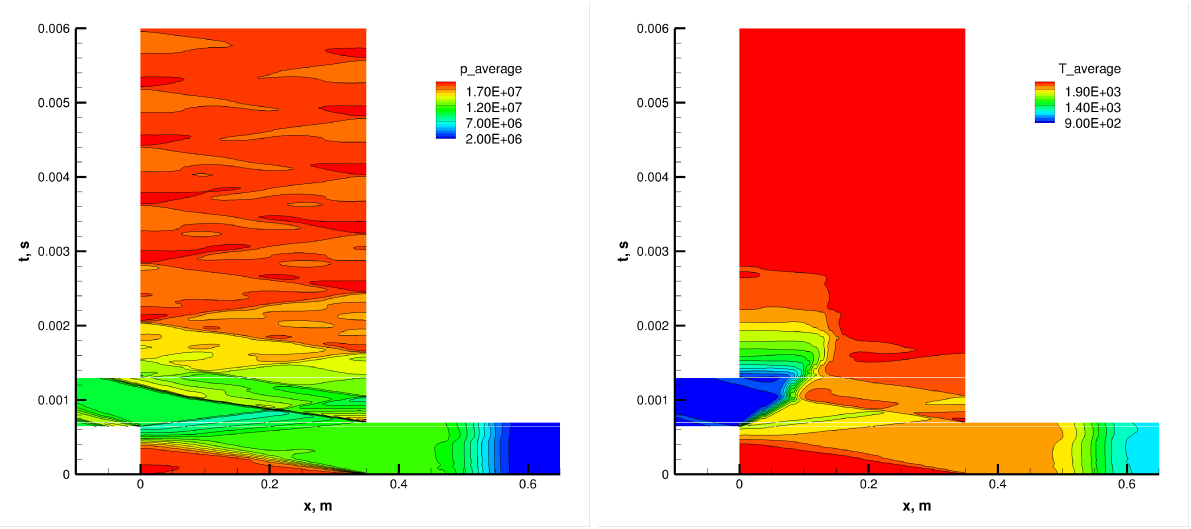

(a) Pressure field.

(b) Temperature field.

Fig 9. Pressure and temperature fields for the reference configuration. Given is the temporal evolution of cross-section-averaged data over one cycle. Inflow and outflow reservoirs are shown during opening times of the corresponding ports. The nozzle in the outflow reservoir is located at a position between $0.5\,m$ to $0.6\,m$.

5.2. Pollutant formation

In the context of combustion characterised by high pressure and temperature it is interesting to look at the amount of carbon-monoxide and nitric-oxide formation. The chemical reaction scheme by Swithenbank provides this information on the basis of elementary reactions covering the formation of both species.

Figure 11 shows the levels of CO, and NO at the inlet and outlet ports of the wave rotor over the time of one cycle. In general, most visible changes of the mass fractions appear at the opening of the inlet port and in particular in the vicinity of the inlet port. The outlet port is affected little, as combustion products are dominant in this region. This is due to the fact, that the wave rotor is only partially filled with fresh gas and mixing is not considered in the simulations. More realistic simulations, presented later, take reservoirs around the wave rotor into account. These simulations strongly suggest that the flow is not uniform with respect to the streamwise positions in the wave rotor and much more pronounced mixing might occur.

Figure 12 gives an overview of equilibrium species mass fractions for CO, CO_2, H_2O and NO for a pressure of 10 and $20\,MPa$ over a temperature range from 800 to $2200\,K$. The mass fractions obtained during the cycle computation are well in line with the equilibrium compositions. Further, there is little impact of the pressure on the equilibrium compositions obtained. Only at very high temperatures there are noticeable differences for CO_2 and H_2O. More importantly, the NO levels significantly increase with increasing temperature. At a temperature of $2000\,K$ a mass fraction of 0.006 is obtained, which is equivalent to a molar fraction of approximately 0.0056 or $5600\,ppm$. It will be difficult to avoid high temperatures during wave rotor operation. Moreover, this is not even wanted from a thermodynamic efficiency point of view. However, it comes at the price of significant levels of NO in the outflow.

5.3. Implications of wave rotor leakage

For the basic analysis of the wave rotor flow an idealised framework has been presumed. However, in terms of an actual realisation of the concept additional problems arise and must be addressed. One issue of potentially greater importance is the leakage that impacts the flow due to the gap between

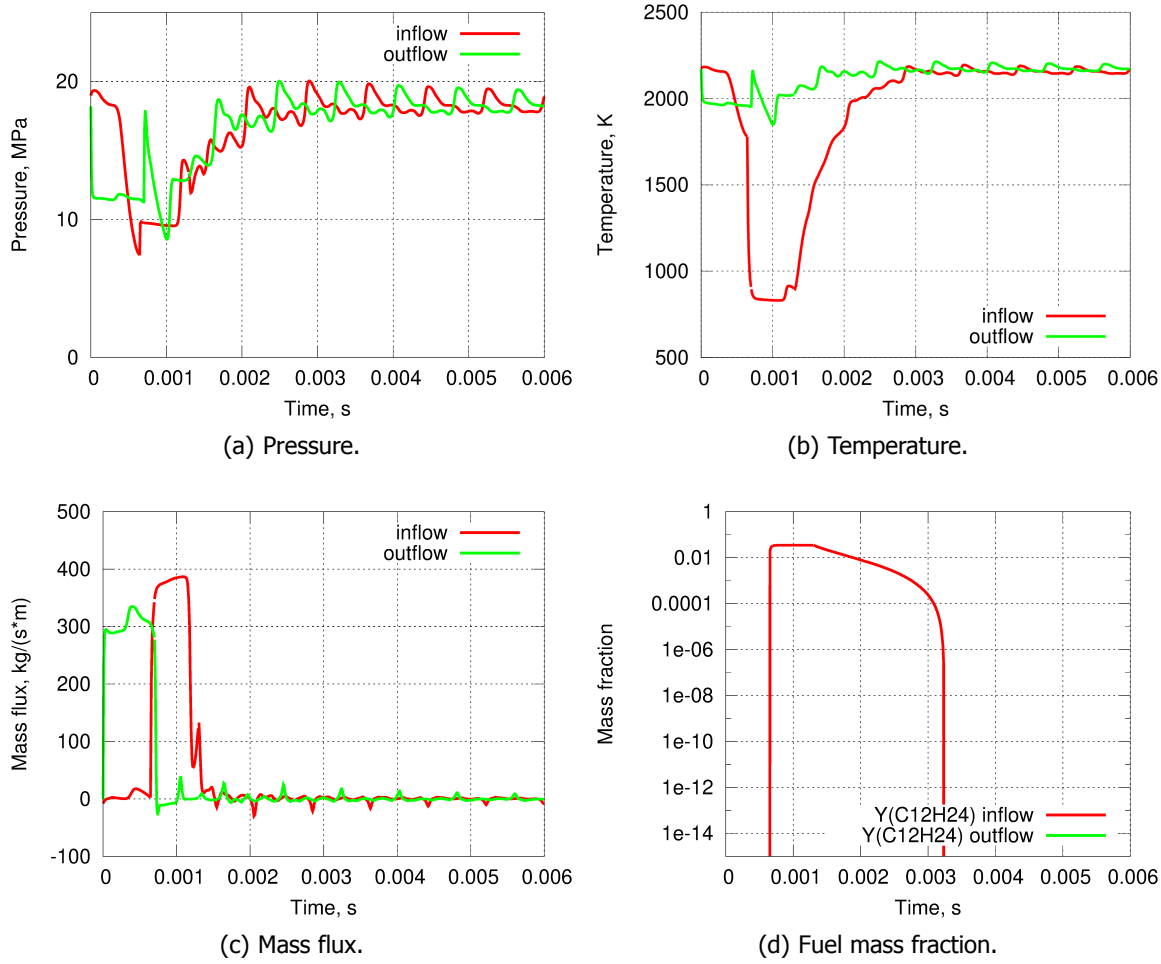

(a) Pressure. (b) Temperature.

(c) Mass flux. (d) Fuel mass fraction.

Fig 10. Pressure, temperature, mass flux and fuel mass fraction at inlet and outlet ports. The values are cross-section averaged at the position of the inlet and outlet ports.

the wave rotor and the surrounding ducts and casings. Thermal expansion of steel can be computed to

$$\Delta L = \epsilon_T \times L \quad \text{with} \quad \epsilon_T = 11 \times 10^{-6} \frac{1}{K} \times \Delta T \tag{4}$$

If the wall temperature increases from initial ambient temperature of $273.15\ K$ to the maximum temperature of $1100\ K$ specified for material in the project TREVAP, an axial expansion of approximately $3.15 \times 10^{-3}\ m$ results for a wave rotor length of $0.35\ m$.

The computations presented in the following presume a gap of $2.5 \times 10^{-3}\ m$ at the beginning and end of the wave rotor. This introduces some margin of safety, which might be considered too narrow from an engineering point of view. At the same time it serves well to illustrate the impact, such a gap around the wave rotor might have on the overall flow and, ultimately, the performance of the wave rotor.

The initial pressure in the configuration is presumed to be the ambient pressure, which is prescribed at the outflow boundary as well. In Fig. 13 the startup process is illustrated in terms of the fuel mass fraction. This resembles the situation at the very beginning, i.e. phase A in the first cycle, where the inflow propagates through the inlet duct and into the wave rotor. Actually, with the reference setup, the incident wave only reaches the wave rotor within phase B. It can be readily observed, that the flow expands into the empty spaces surrounding the wave rotor. Effectively, the supposedly dead spaces

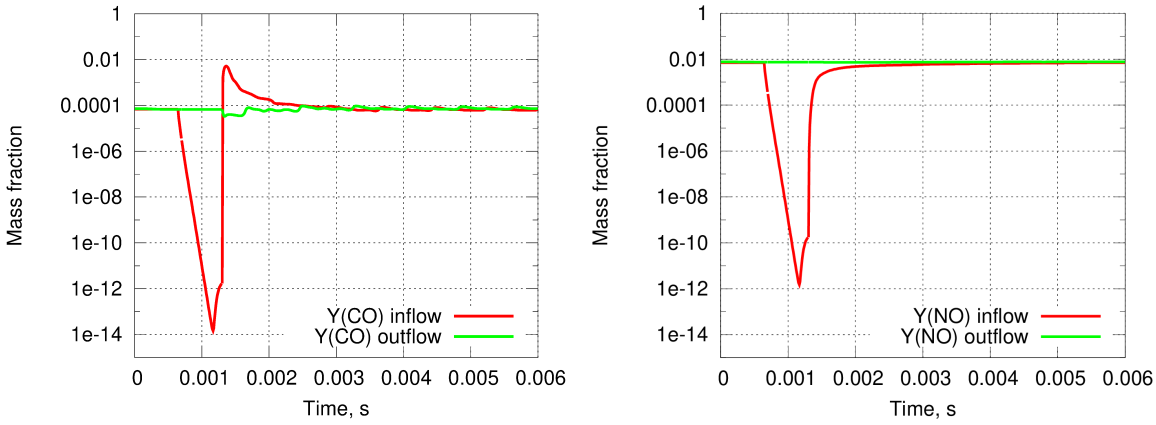

(a) Carbon monoxide.

(b) Nitric oxide.

Fig 11. Species mass fractions of carbon-monoxide and nitric oxide at inlet and outlet ports for the reference configuration. The values are cross-section averaged at the position of the inlet and outlet ports.

around the wave rotor are being filled up with combustible gas mixture! During phase D, where in- and outflow reservoirs are disconnected from the wave rotor, fuel is used up.

The consumption of fuel during phase D yields a significant temperature increase not only in the wave rotor, but in the surroundings of the wave rotor as well. This is shown in Fig. 14 and potentially has a serious impact on the cooling concepts applied to the wave rotor.

During wave rotor operation the pressure level within the surrounding spaces can be expected to be at much higher level than at startup. Nevertheless, the inflow from the compressor will be at a still higher pressure level. Hence, the penetration of fuel into the spaces around the wave rotor will still be an issue not only at startup but during the regular operation, too.

6. Outlook

Pressure gain combustion in a wave rotor was investigated for a given configuration. A sophisticated representation of the chemical reaction is employed, that goes beyond the standard treatment found in the established literature for wave rotors. For the conditions defined, a first understanding of the flow and wave patterns could be gained. Several aspects, such as fuel injection, vaporisation and mixing as well as the impact of the real three-dimensional geometry and rotating components, i.e. the wave rotor, within a fixed engine frame, were not addressed in order to avoid excessive complexity at this state of the work.

Within the overall cycle time of $6\,ms$, almost $4.7\,ms$ were allocated for the constant volume combustion process. This was more than sufficient, because the combustion under the given thermodynamic conditions for the ideally premixed fuel-air mixture only requires $2-3\,ms$. The formation of pollutants was significantly influenced by the high temperatures present in the wave rotor and, therefore, further work will be required for a reduction of, e.g., nitric oxide.

In the context of a real engine operation the issue of leakage was found to be of potentially high importance, as the fuel-air mixture can penetrate into the areas around the wave rotor and cause problems with thermal load due to combustion.

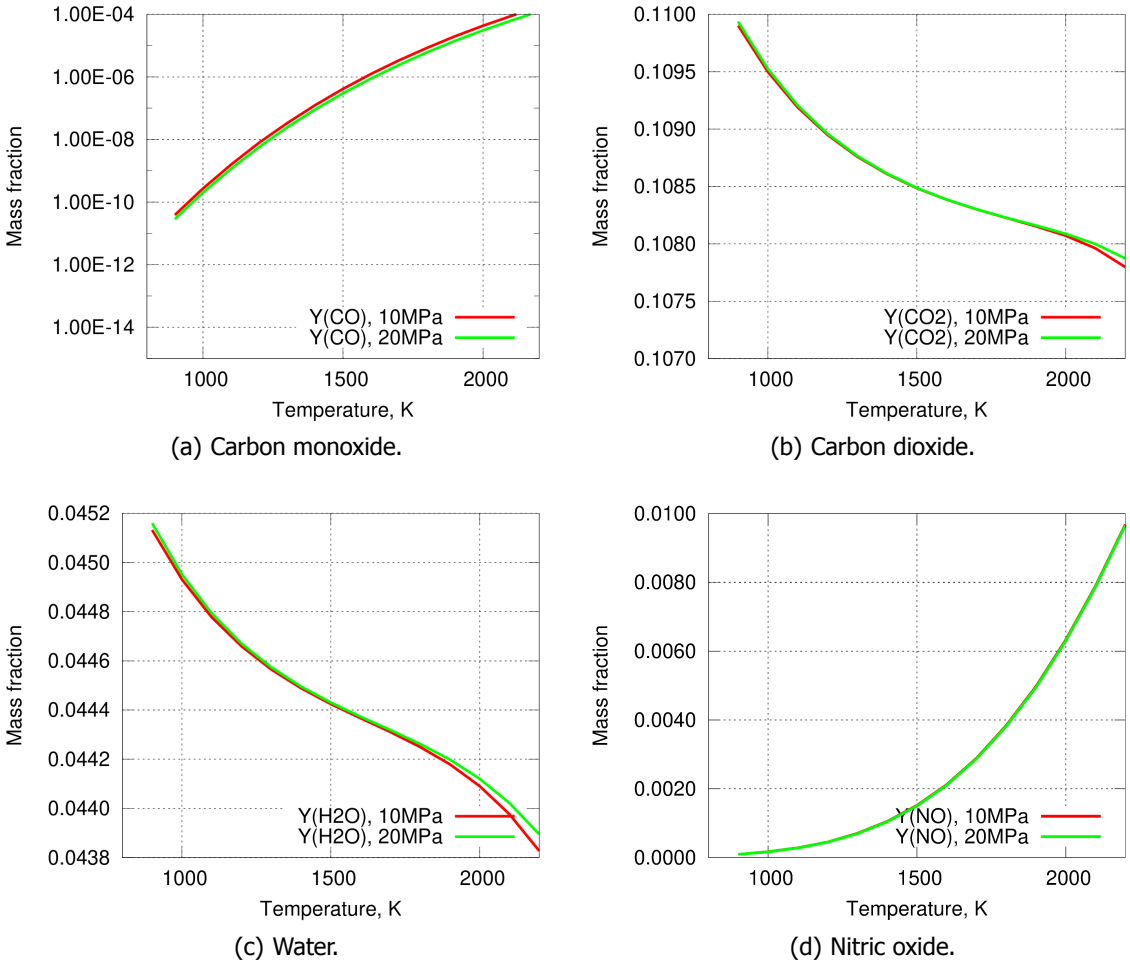

(a) Carbon monoxide.

(b) Carbon dioxide.

(c) Water.

(d) Nitric oxide.

Fig 12. Equilibrium species mass fractions over a temperature range from 800 to $2200\ K$

Acknowledgements

The work was performed within the LUFO V project TREVAP (**T**echnologien für **Rev**olutionäre **A**rbeits-**p**rozesse, project 20E1505F). The author gratefully acknowledges the funding by German Federal Ministry for Economic Affairs and Energy (BMWi).

References

[1] Swithenbank, J., Turan, A., Felton, P. G. and Spalding, D. B., *Fundamental Modelling of Mixing, Evaporation and Kinetics in Gas Turbine Combustion*, AGARD-CP-275, 1979

[2] Wang, T.-S., *Thermophysics Characterization of Kerosene Combustion*, Journal of Thermophysics and Heat Transfer 15(2):140–147, 2001

[3] Slavinskaya, N. A., Riedel, U., Dworkin, S.B. and Thomson, M.J., *Detailed Numerical Modeling Of PAH Formation And Growth In Non-Premixed Ethylene And Ethane Flames*, Combustion and Flame 159:979–995, 2012

[4] Nalim, M. R., Li, H. and Akbari, P., *Air-Standard Aerothermodynamic Analysis of Gas Turbine Engines With Wave Rotor Combustion*, Journal of Engineering for Gas Turbines and Power 131:054506-1, 2009

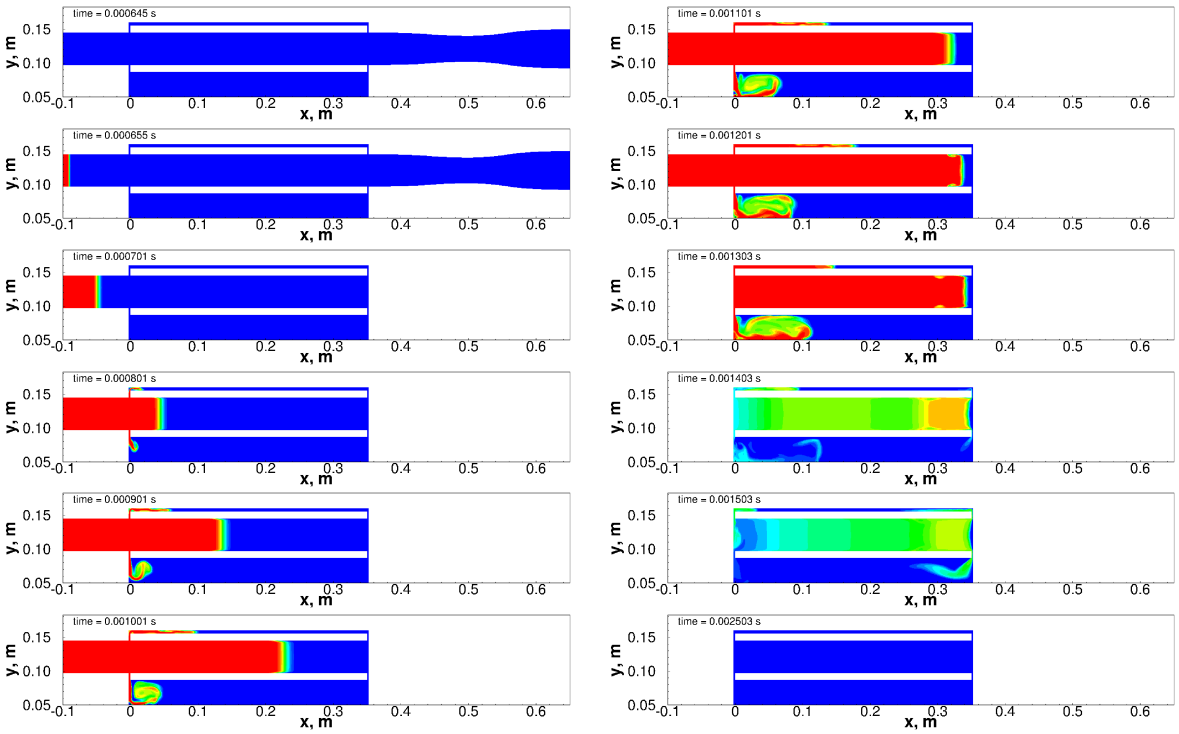

Fig 13. Temporal evolution of fuel inflow to the wave rotor at startup. Inlet and outlet reservoirs are shown when the corresponding ports are open.

[5] Li, H., Akbari, P., Nalim, M. R., *Air-Standard Aerothermodynamic Analysis of Gas Turbine Engines With Wave Rotor Combustion*, AIAA-2007-5050, 2007

[6] Nalim, M. R., *Assessment of Combustion Modes for Internal Combustion Wave Rotors*, Journal of Engineering for Gas Turbines and Power 121:265–271, 1999

[7] Akbari, P., Nalim, M. R., Mueller, N., *A Review of Wave Rotor Technology and Its Applications*, Journal of Engineering for Gas Turbines and Power, 128:717–735, 2006

[8] Nalim, M. R. and Paxson, D. E., *A Numerical Investigation of Premixed Combustion in Wave Rotors*, Journal of Engineering for Gas Turbines and Power 119:668–675, 1997

[9] Paxson, D. E., *A General Numerical Model for Wave Rotor Analysis*, NASA TM 105740, 1992

[10] McBride, B. J. and Gordon, S. and Reno, M. A., *Coefficients for Calculating Thermodynamic and Transport Properties of Individual Species*, NASA TM 4513, 1993

[11] Goos, E., Burcat, A. and Ruscic, B., *Extended Third Millenium Ideal Gas and Condensed Phase Thermochemical Database for Combustion with Updates from Active Thermochemical Tables*, Provided by Elke Goos and available for scientific use from http://burcat.technion.ac.il/dir/ or from http://www.dlr.de/vt/en/desktopdefault.aspx/tabid-7603/12862_read-32379/, 2016

[12] Hirschfelder, J. O. and Curtiss, C. F. and Bird, R. B., *Molecular Theory of Gases and Liquids*, John Wiley & Sons, 1954

[13] Gardiner, W. C., *Combustion Chemistry*, Springer, 1984

[14] Chae, K. *Mass Diffusion and Chemical Kinetic Data for Jet Fuel Surrogates*, PhD Thesis, University of Michigan, 2010

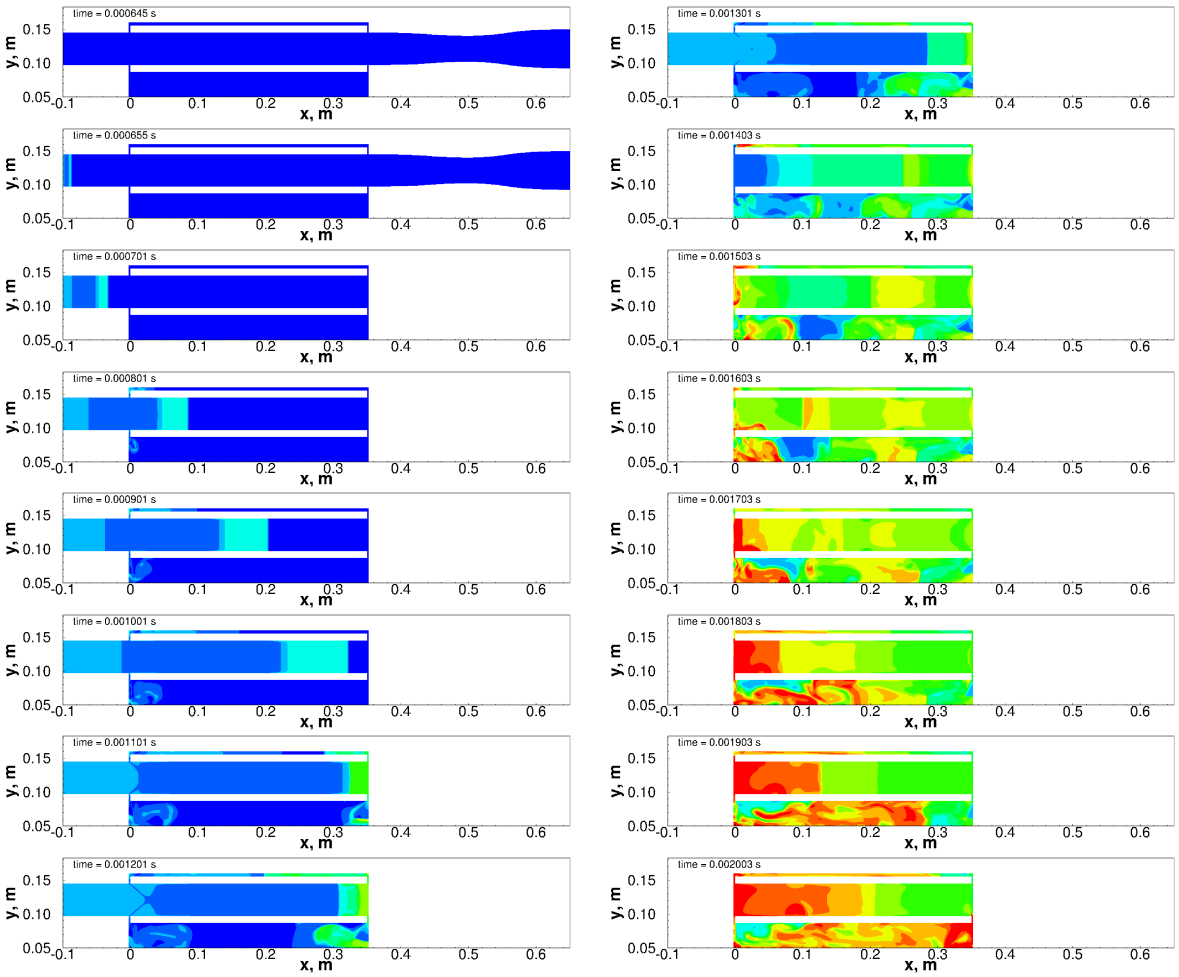

Fig 14. Temporal evolution of temperature in the wave rotor at startup. Inlet and outlet reservoirs are shown when the corresponding ports are open.

[15] Simmie, J. M., *Detailed chemical kinetic models for the combustion of hydrocarbon fuels*, Progress in Energy and Combustion Science, 29:599–634, 2003

[16] Dagaut, P. and Cathonnet, M., *The ignition, oxidation, and combustion of kerosene: A review of experimental and kinetic modelling*, Progress in Energy and Combustion Science, 32:48–92, 2006

[17] Lefebvre, A., Freeman, W. and Cowell, L., *Spontaneous Ignition Delay Characteristics of Hydrocarbon Fuel/Air Mixtures*, NASA-CR-175064, 1986

[18] Chatzianagnostou, D., *Private communication within project TREVAP - reference configuration*, Institute of Aircraft Propulsion Systems, University of Stuttgart, Germany, 2017.